

PAPER • OPEN ACCESS

Frequency dependent wave routing based on dual-band valley-Hall topological photonic crystal

To cite this article: Guo-Chao Wei *et al* 2021 *New J. Phys.* **23** 023029

View the [article online](#) for updates and enhancements.

You may also like

- [Valleytronics in two-dimensional magnetic materials](#)
Chaobo Luo, Zongyu Huang, Hui Qiao et al.
- [Topological phononic metamaterials](#)
Weiwei Zhu, Weiyin Deng, Yang Liu et al.
- [Dc and ac transport in silicene](#)
V Vargiamidis, P Vasilopoulos and G-Q Hai



PAPER

Frequency dependent wave routing based on dual-band valley-Hall topological photonic crystal

OPEN ACCESS

RECEIVED

30 October 2020

REVISED

25 January 2021

ACCEPTED FOR PUBLICATION

4 February 2021

PUBLISHED

18 February 2021

Original content from
this work may be used
under the terms of the
[Creative Commons
Attribution 4.0 licence](#).

Any further distribution
of this work must
maintain attribution to
the author(s) and the
title of the work, journal
citation and DOI.

Guo-Chao Wei^{1,2}, Zhen-Zhen Liu^{1,2}, Da-Sen Zhang^{1,2} and Jun-Jun Xiao^{1,2,*} ¹ Shenzhen Engineering Laboratory of Aerospace Detection and Imaging, Harbin Institute of Technology (Shenzhen), Shenzhen 518055, People's Republic of China² College of Electronic and Information Engineering, Harbin Institute of Technology (Shenzhen), Shenzhen 518055, People's Republic of China

* Author to whom any correspondence should be addressed.

E-mail: eiexiao@hit.edu.cn**Keywords:** valley-Hall topological photonic crystal, valley edge states, frequency dependent wave routing, dual-band**Abstract**

Previous studies on the propagation direction of valley topological edge states mainly focus on the matching between orbital angular momentum of the excitation source and specific pseudo-spin state of valley edge mode at certain frequency that falls in the bandgap of the topologically distinct bulk components. In this work, we propose topological photonic crystals (PCs) hosting two topological protected bandgaps. It is shown that by constructing the interface between different PC structures with distinct topological phase, edge states can be engineered inside these two bandgaps, which provides a convenient way to achieve flexible wave routing. Particularly, we study three types of meta-structures consisting of these PCs in which the valley edge states routing path highly depends on the operating frequency and inputting port of the excitation source. Our study provides an alternative way in designing topological devices such as wave splitters and frequency division devices.

1. Introduction

It is well-known that waves propagating in the conventional photonic crystal (PC) waveguides suffer considerable scattering loss when they pass through sharp bends or small barriers, which greatly limits its application. Recently, topological PCs have attracted tremendous attention due to their intriguing properties such as topological edge states which are unidirectional [1–4], robust against perturbation [5–8] and backscattering immune [9–11] and corner states with high quality factor [12]. These fascinating properties can be realized by constructing a domain wall and corners with artificial structures hosting different topological invariant [13–19]. Topological edge state was first observed in a square lattice composed of gyromagnetic cylinders, in which the band degeneracy point can be lifted by breaking the time-reversal symmetry with external magnetic fields [1]. As such, robust edge states that are immune to the structures disorder and optical obstacles can be realized. However, in optical frequencies, it is difficult to find materials with larger magneto-optical effects. Subsequent research has demonstrated that in time-reversal symmetric systems the degeneracy points can be lifted by breaking the spatial symmetry (e.g. rotation and inversion symmetry) of the structures [20–24]. Hence, topological boundary states can be easily implemented by these meta-structures with different topological invariant in various frequency ranges (e.g. microwave, terahertz and optical frequencies) [25–29].

Dirac points appear at K/K' point in the reciprocal space of a hexagon lattice obeying C_6 or C_{3v} rotation symmetry. By reducing the lattice symmetry to C_3 , the Dirac points would be lifted with energy bands inversion [20]. In this case, Berry curvature in reciprocal space exhibits a pair of energy extrema with different sign at K/K' points, termed as valley [30–32]. The topological invariant in valley-Hall PCs (valley Chern number) can be calculated by integrating the Berry curvature over the half irreducible Brillouin zone (BZ), which generally reads $C_v = C_K - C_{K'} = \pm 1$. Valley edge states can be realized by combining two PCs

with distinct valley Chern number [5]. In the past few years, many potential applications have been proposed, such as topological channel intersections [9], topological laser [33–35] and communication chips [36]. Previous studies of wave routing in valley topological PC mainly focus on the orbital angular momentums of the excitation source and the valley polarization of interface states [37]. However, it is difficult to control the routing path when the structure and source are fixed. To circumvent such issue, recently studies have demonstrated that in non-Hermitian systems, by introducing gain and loss, the propagation path of waves can be flexibly controlled by projecting pumping patterns onto the photonic lattice [38]. In addition, we show that meta-structures can be designed by considering three kinds of structures bearing distinct topological phase and it is possible to adjust edge states at different frequencies in the same band gap, with which the wave propagation path becomes switchable by frequency [39]. However, in this case, the frequency-dependent edge states bands fall in the same band gap which is not easy to control.

In this work, we study a more convenient way to realize propagation routing path in dual bandgaps that are naturally separated in frequency. Firstly, we study two kinds of topological PCs with two Dirac points (localize at lower band and higher band) at K/K' points. When reducing the lattice rotation symmetry, two Dirac points can be lifted up giving rise to two bandgaps. By constructing different types of domain walls via these structures, valley edge states can be flexibly controlled at different frequencies within these two bandgaps. In this way, we designed a pseudo-spin selective meta-structures working on the dual band frequencies in which the wave propagation path depends on the pseudo-spin of the valley edge states. Except that, we also demonstrate two types of frequency selective waveguide structures. It is shown that the propagating path of valley edge states can be controlled by adjusting the frequency of excitation source.

2. Result and discussion

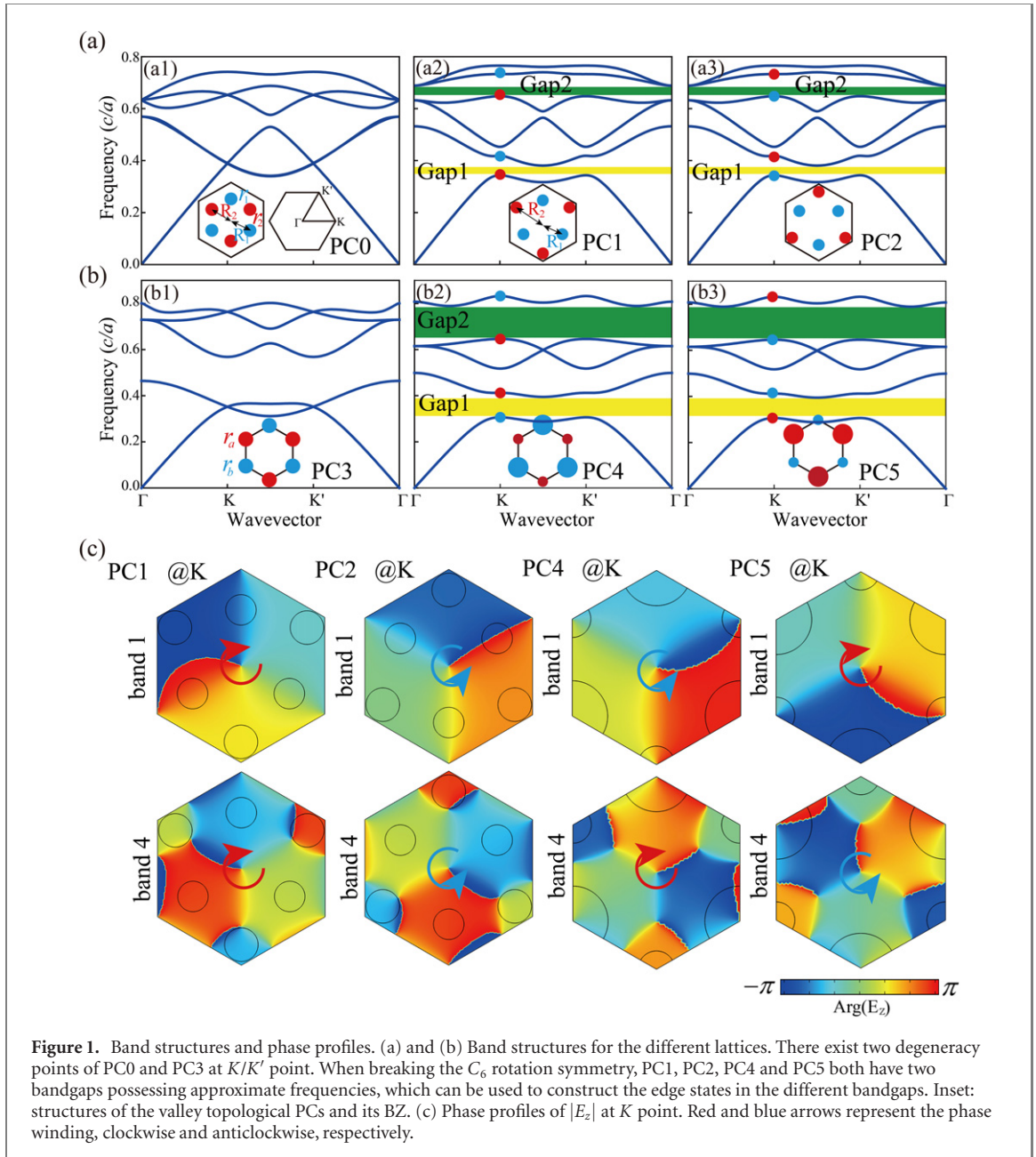
2.1. Band structures of the valley-Hall photonic crystals

The structures of the designed hexagonal PCs are shown in the insets of figures 1(a1) and (b1) which consist of dielectric cylinders array embedded in air background. The relative permittivity of the cylinders is $\varepsilon = 8.9$. The lattice constant is a , and the radii of cylinders in PC0 and PC3 are $r_1 = r_2 = 0.1a$ and $r_a = r_b = 0.16a$, respectively. Notice that we have distinguished the two sublattices which will be utilized to break the lattice symmetry that leads to the topological phase transition. The distances between the lattice center and the cylinder are $R_1 = R_2 = a/3$. Figures 1(a1) and (b1) show the band structures of PC0 and PC3. It is clear that there exist two degeneracy points at the BZ boundaries (K/K' point) at $f = 0.388c/a, 0.635c/a$ and $f = 0.352c/a, 0.765c/a$ due to the C_6 rotation symmetry. In figure 1(a2), by expanding the off-center distance of cylinders 2 (red circles) to $R_2 = a/2.2$ and reducing the radius of cylinders 1 (blue circles) to $r_1 = 0.09a$ (see inset in figure 1(a2)), the lattice symmetry is reduced to C_3 . Then the degeneracy points at K/K' are lifted resulting into two bandgaps (yellow and green regions in figure 1(a2)) spanning respectively from $f = 0.342c/a$ to $f = 0.38c/a$ and $f = 0.648c/a$ to $f = 0.689c/a$. The red and blue dots at K point of the band structure represent pseudospin-down and pseudospin-up states, respectively. When the lattice is rotated by 180° (see inset in figure 1(a3)), the pseudospin states are switched for both the lower and higher bands, indicating that PC1 and PC2 host different topological phases in these two band gaps.

For another case, PC4 (seen inset in figure 1(b2)) is constructed by varying the radius of cylinders on one sublattice in PC3, in which $R_a = 0.11a, R_b = 0.21a$. The corresponding band structures are shown in figure 1(b2). It is clear that the degeneracy points at K/K' are lifted, and two complete band gaps appear from $f = 0.306c/a$ to $f = 0.395c/a$ and $f = 0.646c/a$ to $f = 0.79c/a$ which are consistent with the band gaps in PC1 and PC2. The band structures in figure 1(b3) are calculated for the case of $R_a = 0.21a, R_b = 0.11a$ which resemble PC4. However, their topological indexes are exchanged as discussed in the following.

Based on the $\mathbf{k} \cdot \mathbf{p}$ perturbation theory, the effective Hamiltonian around K/K' valley can be expressed as $H_{K/K'} = \pm(v_D \delta k_x \sigma_x + v_D \delta k_y \sigma_y) \pm m v_D^2 \sigma_z$, in which v_D is the group velocity, $\delta \mathbf{k} = \mathbf{k} - \mathbf{k}_{K/K'}$ is the displacement from the wave vector \mathbf{k} to the K/K' valley in reciprocal space, $\sigma_i (i = x, y, z)$ are the Pauli matrices and m is effective mass term [15]. The nonzero topological index is relative to the sign of effective mass term, $C_{K/K'} = \pm \text{sgn}(m)/2$ and the valley Chern number is calculated as $C_v = C_K - C_{K'}$. During the band inversion around the lower energy band gap (gap 1) and the higher band gap (gap 2), the valley Chern number is changed between 1 and -1 (not show here), highlighting the topological phase transition.

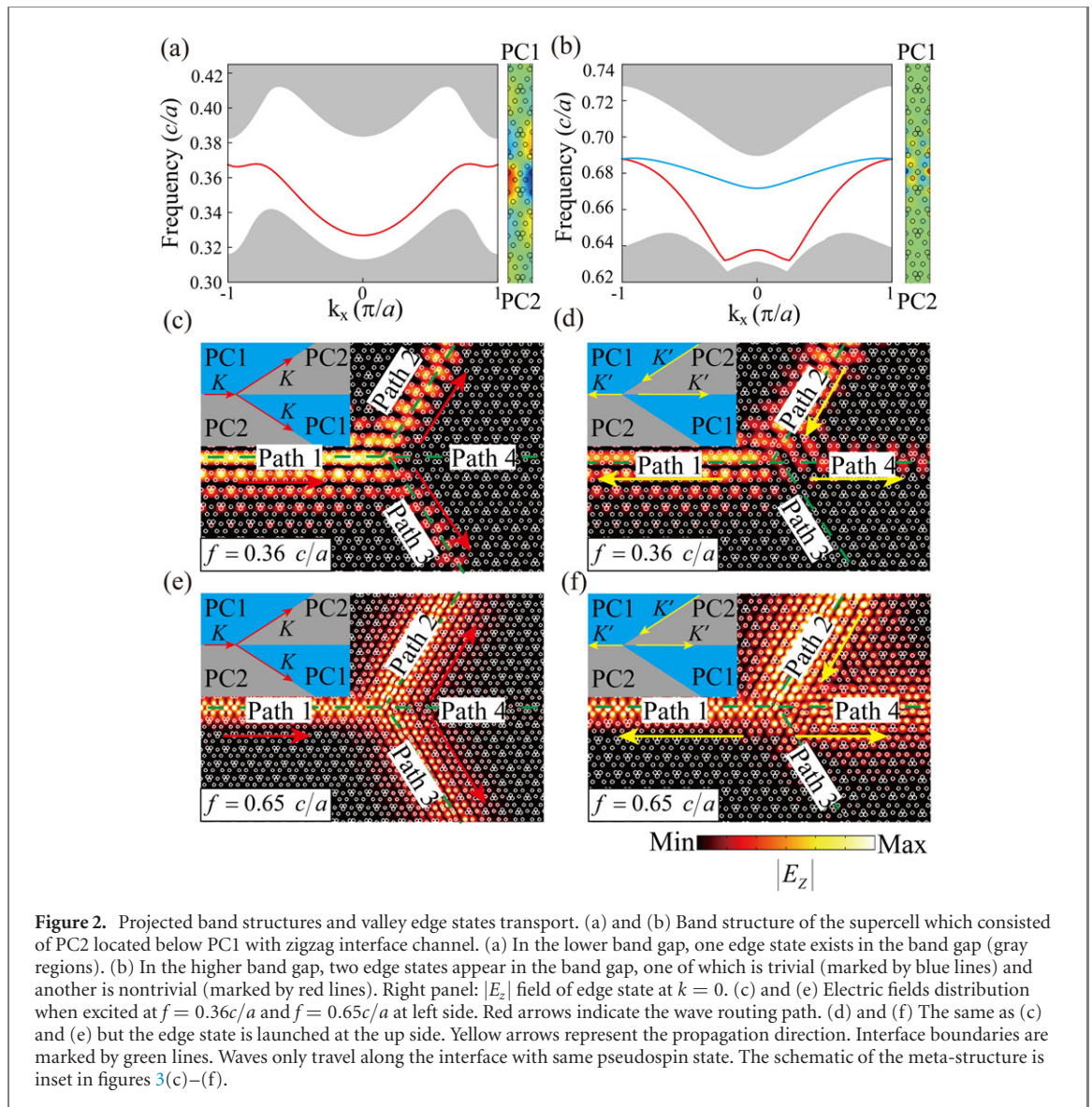
The corresponding phase winding behavior of the eigenmode electric fields ($|E_z|$) at K point are shown in figure 1(c). In this time-reversal symmetric system, it exhibits opposite winding pattern at K' point (not show here). Below the lower band gap, the phase patterns of the eigenmode at the first band are clockwise (red arrow) in PC1, PC5 and anticlockwise (blue arrow) in PC2, PC4 which demonstrate the



different topological index (opposite sign of valley Chern number). Below the higher band gap, the eigenmodes of the fourth band have clockwise and anticlockwise phase winding patterns for PC1, PC4 and PC2, PC5 respectively, indicating the different topological natures of the band gaps between them.

2.2. Dual-band edge states and pseudospin selective edge states transport

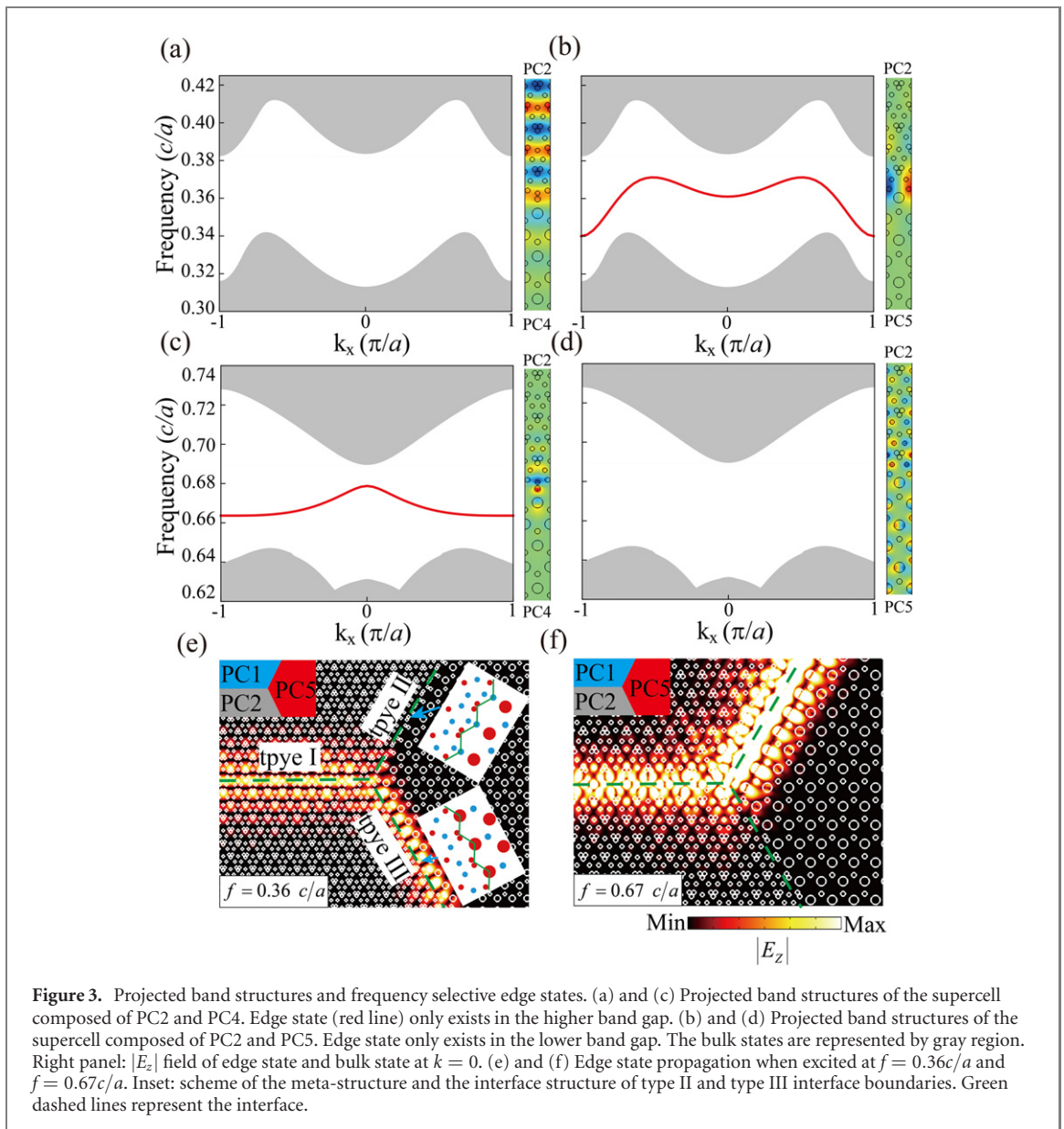
According to the bulk-edge correspondence, edge states can be realized at an interface between two structures with different topological phases. In this section, the interface channels are considered in zigzag shape. Figure 2(a) shows the projected band structures along x -axis for the supercell composed of PC1 and PC2 around the lower band gap. As expected, one edge state (red line) appears inside the band gap between $f = 0.327c/a$ and $f = 0.367c/a$ where the projected bulk bands are represented by the gray regions. The corresponding electric field of the edge state at $k = 0$ is shown in the right panel of figure 2(a). It is clear that the fields are well confined at the interface. Figure 2(b) shows the projected band structures around the higher band gap. Two edge state dispersions appear in the gap, one of which is trivial (blue line) that is similar in reference [40]. The other is nontrivial (red line) covering the frequency range from $f = 0.632c/a$ to $f = 0.688c/a$ which originates from the distinct valley Chern number between the PCs across the interface. Certainly, the electric fields are highly confined at the interface which is exemplified by the field distribution at $k = 0$ in the right panel of figure 2(b).



In order to demonstrate the performance of dual band pseudo-spin selective wave routing, we construct a meta-structure in which PC1 and PC2 are separated alternatively, defining several PC1/PC2 and PC2/PC1 interfaces and four input/output ports. The schematic of the meta-structure is shown in the insets of figures 2(c)–(f). Figure 2(c) shows the $|E_z|$ fields when the source signal with $f = 0.36c/a$ is launched from the left side. The propagation direction is represented by the red arrows. One can see that signals propagate along path 1, then split into path 2 and path 3, with no wave traveling along path 4. Noticeably, the signals in path 2 look stronger than those in path 3. This is mainly due to different coupled efficiency on the channel. Figure 2(e) is basically the same to figure 2(c) but at higher excitation frequency $f = 0.65c/a$. In both cases, the signals smoothly pass through the band corner (120°) with negligible scattering. Interestingly, figures 2(d) and (f) show the cases when the signal is launched from the top port, waves can travel along path 2 and split only to path 1 and path 4, without any energy injected to the path 3. This routing phenomenon is guaranteed by the different valley pseudospin of the interface states. Waves only travel along the path with same pseudospin state when pass through the intersection structures. This can be readily used in beam splitters and wavelength division optical waveguides.

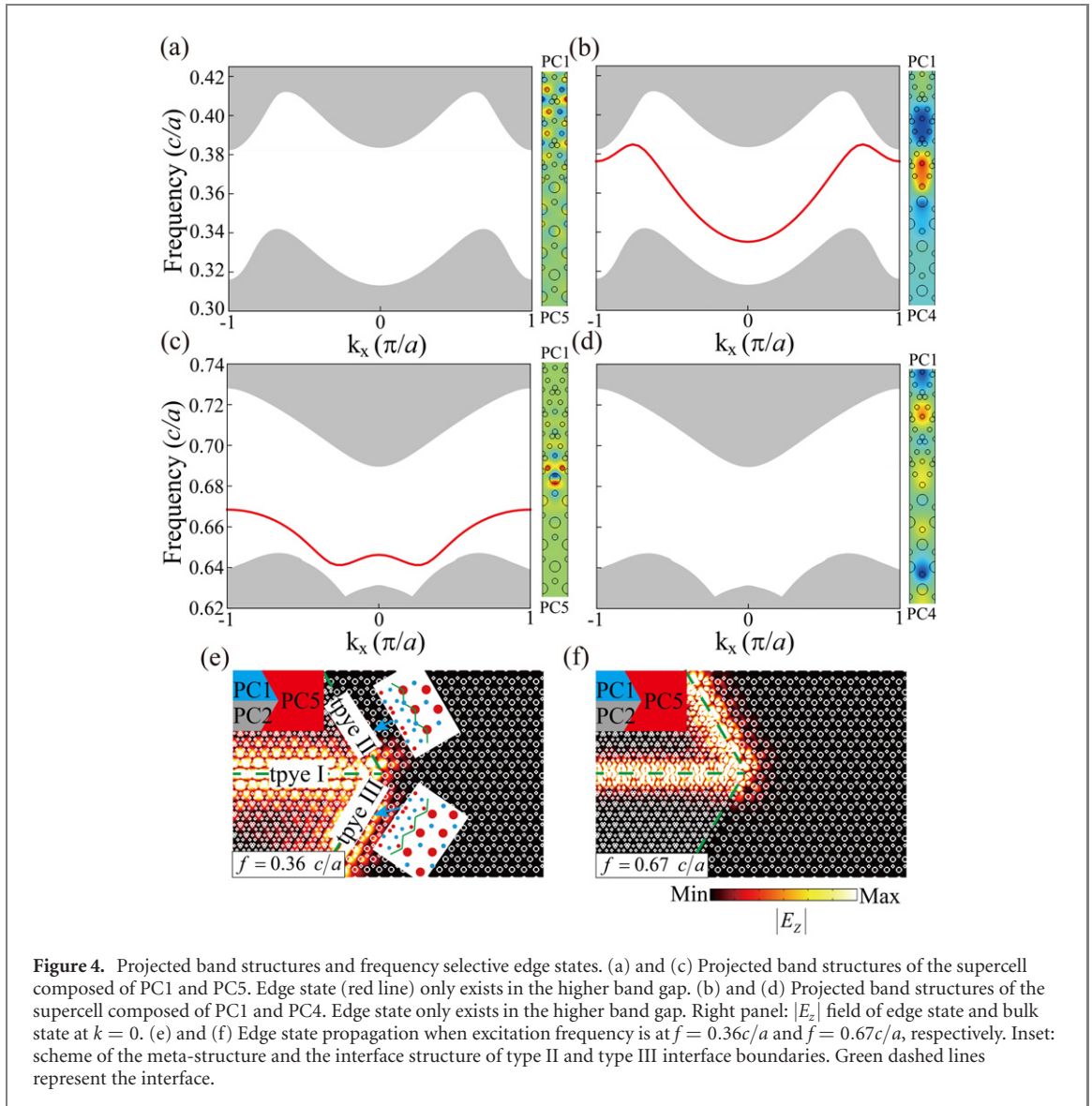
2.3. Frequency selective edge states routing path

Next, we study the edge states routing path with respect to the excitation frequency which is realized by constructing different interfaces with edge states that fall in different bandgaps. As shown in figure 1(c), one can see that for the first band, PC2 and PC4 have the same phase windings at K point while PC2 and PC5 host the opposite phase windings. Thus, in the lower band gap, edge state exists at the interface composed of PC2 and PC5 while no edge state appears at the interface between PC2 and PC4. As for the fourth band,



the phase windings at K point of PC2 and PC5 are anticlockwise, but clockwise for PC4. Therefore, in the higher band gap, topological edge state is supported at the interface composed of PC2 and PC4 but not for the combinations of PC2 and PC5. Above this discussion, figures 3(a) and (c) show the projected band structures of the supercell composed of PC2 and PC4. As expected, edge state only exist inside the higher band gap from $f = 0.663c/a$ to $f = 0.679c/a$. The corresponding electric fields of edge and bulk modes are shown at the right panel. While for the combination between PC2 and PC5, edge state only appears in the lower band gap from $f = 0.34c/a$ to $f = 0.371c/a$, as shown in figures 3(b) and (d). Moreover, for the interface between PC1 and PC2, edge states exist at both band gaps (shown in figures 2(a) and (b)).

In view of such properties, we study a meta-structure composed of PC1, PC2 and PC5, as shown in the insets of figures 3(e) and (f). There are three types of interfaces between different PCs, and the angles between these interfaces are 120° . Note that the edge states for the titled type II and type III interfaces are consisted of PC1, PC2 and PC5. However, along the sloping interface direction, type II and type III interfaces can be viewed as the combination of PC2/PC4 channel and PC2/PC5 channel, respectively (detailed structures can be seen in the insets of lattice geometry in figure 3(e), and the right panels of figures 3(a) and (b)). The corresponding edge states dispersion are already shown in figures 3(a) and (b). Therefore, when the excitation frequency is $f = 0.36c/a$, waves pass through type I interface (by PC1/PC2) smoothly and travel only along the type III interface, as shown in figure 3(e). For the other case, when the excited frequency is $f = 0.67c/a$, wave travels along type I and bends toward type III interface, without any energy coupled to the type II interface, as shown in figure 3(f). All of these can well demonstrate the frequency selective topological wave routing in our meta-structure.



To further study the effect of the angles between these three types of interface channels on the frequency selective wave routing. We construct a new meta-structure which still consists of PC1, PC2 and PC5, as shown in the inset of figures 4(e) and (f). The channel angles between type I, type II and type I, type III are 60° and -60° , respectively. It is worth noting that the structures of tilted type II and type III interface are different with respect to those in figures 3(e) and (f). The details can be seen in the zoom-in pictures (see inset in figure 4(e)). The projected band structures of type II interface are shown in figures 4(a) and (c). Clearly, edge state only appears in the higher band gap spanning from $f = 0.641c/a$ to $f = 0.668c/a$. As for type III interface, the band structures are shown in figures 4(b) and (d). As can be seen, one edge state covering $f = 0.335c/a$ to $f = 0.385c/a$ appears in the lower band gap and no edge state is found in the higher band gap. The corresponding eigenmode electric fields of edge and bulk states at $k = 0$ are shown in the right panels.

Figure 4(e) shows the wave routing path when the excitation frequency is $f = 0.36c/a$. As expected, the excitation waves travel along type I interface and then turn to the type III interface which agree well with the edge states dispersion in figures 4(a) and (b). When the operating frequency is switched to $f = 0.67c/a$, the excitation wave travels along type I interface and is then guided toward the type II interface, with the bending angle 120° , as shown in figure 4(f).

2.4. Robustness analysis of wave routing

One of the most intriguing properties of topological edge states is their robustness to the perturbations. Here, we demonstrate the robust transport of wave routing by introducing some defects and disorders around the interface. Figure 5(a) shows the electric fields distribution at $f = 0.36c/a$ whose structure is the

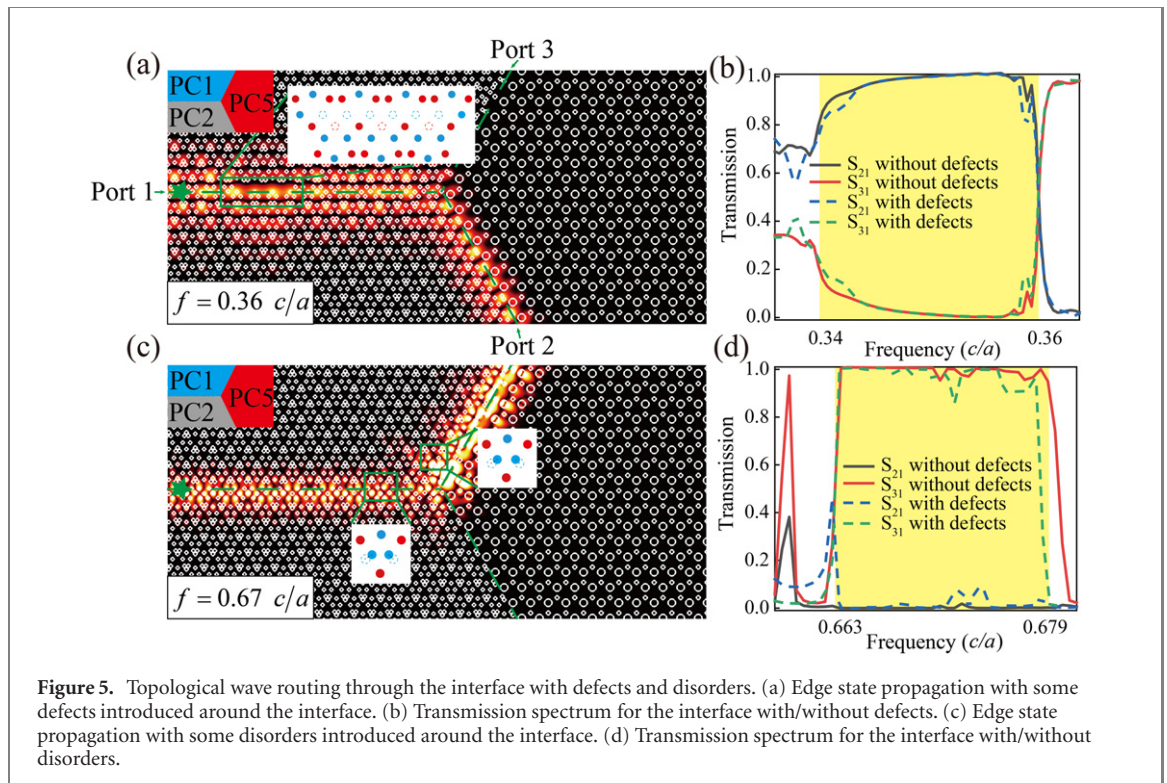


Figure 5. Topological wave routing through the interface with defects and disorders. (a) Edge state propagation with some defects introduced around the interface. (b) Transmission spectrum for the interface with/without defects. (c) Edge state propagation with some disorders introduced around the interface. (d) Transmission spectrum for the interface with/without disorders.

same to figure 3(e) but with some defects (see zoom-in picture) introduced around the interface. The excitation source is represented by the green star. As can be seen, waves smoothly pass through the defects with negligible back-scattering. The corresponding transmission spectrum is shown in figure 5(b). By comparison, we remark that the small defects have little effect on the transmission efficiency. In addition, in our 2D dielectric system, there is no absorption and radiation loss, and the main reason affecting transmission efficiency is the back-scattering which is mainly due to the edge states phase mismatch between PC1, PC2 and PC2, PC5. As for the higher frequency, figure 5(c) shows the electric fields excited by the source with $f = 0.67c/a$, whose structure is same to figure 3(f) but with some disorders around the interface. Simultaneously, the corresponding transmission spectrum is shown in figure 5(d). The results indicate that the wave routing structures in our work have well robustness for the small perturbation.

3. Discussion and conclusion

The topological waveguides are useful in many on chip integrated optical devices and the robustness of edge states is crucial. However, in time-invariant photonic topological insulators, the edge states are not perfectly unidirectional, thus the specific perturbation might deteriorate the waves propagation (back-scattering). In such case, the robustness of wave propagation can be optimized by increasing the group velocity of edge state dispersion [41, 42]. That can be accomplished by traditional optimization methods or machine learning based approaches [43, 44].

In summary, we have designed two topological PCs made of arrayed cylinders in C_6 rotation symmetry hosting Dirac points at K point in both low and high energy bands. By adjusting the position and radii of the cylinders, the Dirac points are lifted, yielding two complete band gaps accompanied with topological phase transition. Valley edge states can be realized by constructing an interface between these structures hosting different topological phase. Via combining these structure in 2D plane, we demonstrate the meta-structures consisted a diversity of such PCs exhibit topologically protected wave propagating path, heavily depending on the interface type, as well as the frequency of the excitation source. Our results can also be designed in the photonics crystal slab system which can be used in optical waveguides [7], frequency division devices [39] on chip optical communication [36].

Acknowledgments

This work was financially supported by the Shenzhen Municipal Science and Technology Plan (Nos. JCYJ20180306172003963 and JCYJ 20170811154119292).

Data availability statement

All data that support the findings of this study are included within the article (and any supplementary files).

ORCID iDs

Jun-Jun Xiao  <https://orcid.org/0000-0002-8972-013X>

References

- [1] Wang Z, Chong Y, Joannopoulos J D and Soljačić M 2009 *Nature* **461** 772
- [2] Wu X, Meng Y, Tian J, Huang Y, Xiang H, Han D and Wen W 2017 *Nat. Commun.* **8** 1304
- [3] Kang Y, Ni X, Cheng X, Khanikaev A B and Genack A Z 2018 *Nat. Commun.* **9** 3029
- [4] Ni X, He C, Sun X-C, Liu X-P, Lu M-H, Feng L and Chen Y-F 2015 *New J. Phys.* **17** 053016
- [5] Ma T and Shvets G 2016 *New J. Phys.* **18** 025012
- [6] He C, Ni X, Ge H, Sun X-C, Chen Y-B, Lu M-H, Liu X-P and Chen Y-F 2016 *Nat. Phys.* **12** 1124
- [7] Shalaev M I, Walasik W, Tsukernik A, Xu Y and Litchinitser N M 2019 *Nat. Nanotechnol.* **14** 31
- [8] Xie X, Li H, Peng Y, Zhu X, Luo W and Zhao D 2019 *New J. Phys.* **21** 073047
- [9] Zhang L et al 2019 *Laser Photon. Rev.* **13** 1900159
- [10] Ma J, Xi X and Sun X 2019 *Laser Photon. Rev.* **13** 1900087
- [11] Chen X D, He X T and Dong J W 2019 *Laser Photon. Rev.* **13** 1900091
- [12] Ota Y, Liu F, Katsumi R, Watanabe K, Wakabayashi K, Arakawa Y and Iwamoto S 2019 *Optica* **6** 786
- [13] Proctor M, Craster R V, Maier S A, Giannini V and Huidobro P A 2019 *ACS Photon.* **6** 2985
- [14] Zhang Z, Tian Y, Wang Y, Gao S, Cheng Y, Liu X and Christensen J 2018 *Adv. Mater.* **30** 1803229
- [15] Chen Q, Zhang L, He M, Wang Z, Lin X, Gao F, Yang Y, Zhang B and Chen H 2019 *Adv. Opt. Mater.* **7** 1900036
- [16] Wu X et al 2019 *Adv. Opt. Mater.* **7** 1900872
- [17] Wei G, Liu Y, Liu Z, Zhang D and Xiao J 2020 *J. Phys. D: Appl. Phys.* **53** 435104
- [18] Liu Z, Zhang Q, Qin F, Zhang D, Liu X and Xiao J J 2019 *Phys. Rev. B* **99** 085441
- [19] He X-T, Liang E-T, Yuan J-J, Qiu H-Y, Chen X-D, Zhao F-L and Dong J-W 2019 *Nat. Commun.* **10** 872
- [20] Lu J, Qiu C, Xu S, Ye Y, Ke M and Liu Z 2014 *Phys. Rev. B* **89** 134302
- [21] Lee T and Iizuka H 2019 *Phys. Rev. B* **99** 064305
- [22] Zhang Z, Tian Y, Cheng Y, Wei Q, Liu X and Christensen J 2018 *Phys. Rev. Appl.* **9** 034032
- [23] Darabi A and Leamy M J 2019 *Phys. Rev. Appl.* **12** 044030
- [24] Miniaci M, Pal R K, Morvan B and Ruzzene M 2018 *Phys. Rev. X* **8** 031074
- [25] Shalaev M I, Walasik W and Litchinitser N M 2019 *Optica* **6** 839
- [26] Jung M, Gladstone R G and Shvets G 2020 *Adv. Photon.* **2** 046003
- [27] Shen Y, Qiu C, Cai X, Ye L, Lu J, Ke M and Liu Z 2019 *Appl. Phys. Lett.* **114** 023501
- [28] Mei J, Wang J, Zhang X, Yu S, Wang Z and Lu M-H 2019 *Phys. Rev. Appl.* **12** 054041
- [29] Gao M, Wu S and Mei J 2020 *New J. Phys.* **22** 013016
- [30] Dong J-W, Chen X-D, Zhu H, Wang Y and Zhang X 2017 *Nat. Mater.* **16** 298
- [31] Yan M, Lu J, Li F, Deng W, Huang X, Ma J and Liu Z 2018 *Nat. Mater.* **17** 993
- [32] Lu J, Qiu C, Ye L, Fan X, Ke M, Zhang F and Liu Z 2016 *Nat. Phys.* **13** 369
- [33] Harari G, Bandres M A, Lumer Y, Rechtsman M C, Chong Y D, Khajavikhan M, Christodoulides D N and Segev M 2018 *Science* **359** 1230
- [34] Bandres M A, Wittek S, Harari G, Parto M, Ren J, Segev M, Christodoulides D N and Khajavikhan M 2018 *Science* **359** 1231
- [35] Noh W, Nasari H, Kim H-M, Le-Van Q, Jia Z, Huang C-H and Kanté B 2020 *Opt. Lett.* **45** 4108
- [36] Yang Y, Yamagami Y, Yu X, Pitchappa P, Webber J, Zhang B, Fujita M, Nagatsuma T and Singh R 2020 *Nat. Photon.* **14** 446
- [37] Yang Y, Jiang H and Hang Z H 2018 *Sci. Rep.* **8** 1588
- [38] Zhao H, Qiao X, Wu T, Midya B, Longhi S and Feng L 2019 *Science* **365** 1163
- [39] Wei G, Liu Z, Liu Y, Zhang D and Xiao J 2020 *Opt. Lett.* **45** 5608
- [40] Orzabayev B and Fleury R 2019 *Nanophotonics* **8** 1433
- [41] Arregui G, Gomis-Bresco J, Sotomayor-Torres C M and Garcia P D 2021 *Phys. Rev. Lett.* **126** 027403
- [42] Yoshimi H, Yamaguchi T, Ota Y, Arakawa Y and Iwamoto S 2020 *Opt. Lett.* **45** 2648
- [43] Minkov M, Williamson I A D, Andreani L C, Gerace D, Lou B, Song A Y, Hughes T W and Fan S 2020 *ACS Photon.* **7** 1729
- [44] Chen Y, Meng F, Kivshar Y, Jia B and Huang X 2020 *Phys. Rev. Res.* **2** 023115